Available online at www.sciencedirect.com

ScienceDirect

Procedia Engineering 133 (2015) 348 – 361

Procedia Engineering

www.elsevier.com/locate/procedia

6th Fatigue Design conference, Fatigue Design 2015

Fatigue crack growth under constant and variable amplitude loading at semi-elliptical and V-notched steel specimens

David Simunek[a]*, Martin Leitner[a], Jürgen Maierhofer[b], Hans-Peter Gänser[b]

[a]*Montanuniversität Leoben, Franz-Josef-Straße 18, 8700 Leoben, Austria*
[b]*Materials Center Leoben Forschung GmbH, Roseggerstraße 12, 8700 Leoben, Austria*

Abstract

An assessment of fatigue crack propagation in components and structures based on fracture mechanical approaches is fundamental to define periodic intervals for service inspections. This paper focuses on the investigation of flat specimens made of mild steel S355 with V-shaped and semi-elliptical notches under constant and variable amplitude fatigue loading to analyze the influence of load sequence effects on crack propagation in order to obtain information about the remaining service life of components. Depending on the load sequence, crack propagation may be accelerated, delayed or in some cases even stopped, which leads to beach marks within the area of fracture. Fractographic analyses of the tested specimens are carried out by light-optical microscopy to determine different crack propagation stages. Numerical and analytical linear-elastic fracture mechanics (LEFM) calculations based on two- and three-dimensional models are performed for constant and variable amplitude loads. All analytical assessments of the V-notched specimen illustrate conservative results compared to testing, and the numerical results match the experimental investigations well. The maximum deviation of results is observed at variable amplitude loading due to missing retardation effects for the LEFM calculations. Preliminary distortion measurements and application of strain gauges on semi-elliptical notched specimens are performed to investigate the influence of angular deformation due to clamping on the local stress distribution. A simple model accounting for superimposed static bending stresses due to clamping is able to improve the crack growth predictions for semi-elliptical surface cracks significantly. A final comparison of the fractographic analyses and the numerical crack propagation calculations illustrates differences in the results and provides information to assess the fatigue crack growth and service inspection intervals of components under variable amplitude loading more precisely.

Peer-review under responsibility of CETIM

Keywords: Fatigue crack propagation; variable amplitude loading; load sequences; lifetime assessment; inspection intervals.

Peer-review under responsibility of CETIM
doi:10.1016/j.proeng.2015.12.670

1. Introduction

Crack propagation at constant amplitude loading in cyclically loaded structures is hardly found in most practical applications. Several crack propagation models, like the Paris law [1] or the crack growth equation according to Forman/Mettu [2], describe the crack propagation rate at constant amplitude loading conditions. Recently, crack growth models accounting for the somewhat strange behavior of physically short cracks under constant amplitude loading have been proposed, e.g. [3]. In comparison to constant amplitude loading, variable amplitude loading often leads to load sequence effects, which may cause acceleration, retardation or arrest of crack propagation. These phenomena are dependent on the block load ratio, stress ratio and the kind of load sequence (low-high or high-low) [4]. In [5-9] investigations of load interaction effects on fatigue crack growth are presented. In many experimental investigations retardation of crack growth after an overload can be observed, which can affect total lifetime significantly. The overload effect depends on the baseline stress intensity factor (SIF) range, the overload ratio and the number of overload cycles. The reason for these phenomena is explainable through an interaction of crack closure effects, crack tip blunting, strain hardening and residual stresses at the crack tip [8]. In this paper, results of fatigue crack growth tests at constant and variable amplitude loads for two different types of specimens are presented. The effect of alternating stress levels on crack propagation rate and remaining service life is analyzed. An indirect potential drop method is used to measure the crack length during testing. Additionally, strain gauge measurements are made to consider clamping stresses, arising from distortion of the specimen, on fatigue crack growth. Fractography is performed to investigate different stages of crack propagation. The experimental results are compared to predictions from numerical and analytical crack propagation assessment methods.

Nomenclature

a	Crack depth
a/c	Crack aspect ratio
Δa	Crack increment
C	Crack growth rate coefficient
CAL	Constant amplitude loading
c	Surface crack half length
$\mathrm{d}a/\mathrm{d}N$	Crack growth rate
F_s	Geometry function
H	Geometry function
K_{IC}	Critical stress intensity factor
K_{min}	Minimal stress intensity factor
K_{max}	Maximum stress intensity factor
ΔK	Stress intensity factor range
ΔK_{th}	Threshold stress intensity factor range
$\Delta K_{th,0}$	Threshold stress intensity factor range for R = 0
m	Crack growth rate exponent
Q	Geometry function
R	Stress ratio
R_b	Block load ratio
SIF	Stress intensity range
σ_a	Stress amplitude
σ_{ben}	Shell bending stress
σ_{mem}	Membrane stress
$\Delta\sigma$	Stress amplitude range
t	Thickness of specimen
VAL	Variable amplitude loading
W	Width of specimen

2. Experimental investigations

Experimental investigations on flat test pieces under fatigue loading are conducted to determine crack growth parameters and to analyze crack propagation. Therefore, two different types of specimens with a width of W = 50 mm and a thickness of t = 12 mm are manufactured. The contour of both specimens is water jet cut and the notches are machined by spark erosion. Fatigue crack growth tests are carried out under constant and variable stress amplitude loading at a constant load stress ratio of R = 0 (pulsating loading). As base material, a ductile construction steel S355 is used. A literature review of preliminary investigations regarding crack propagation parameters for construction steels is conducted to estimate remaining service life and to specify a test plan, see Table 1. The indirect potential drop method is applied to observe crack propagation, and strain gauge measurements are performed to determine the static stresses, induced by distortion due to the clamping process and the local stress distribution during fatigue testing. For the indirect potential drop method a crack gauge containing an electrically conductive coating is applied at the starter notch of the specimen. During crack propagation, the gauge is being torn apart in the same way as the crack extends across the surface. The rising electric resistance of the crack gauge allows to determine the crack extension during testing. The crack gauges are connected to the measuring system FRACTOMAT [10], which includes a highly accurate voltmeter.

Table 1. Summary of crack propagation parameters from literature

Literature	C [mm/cycle]	m [-]	ΔK_{th} [MPa mm$^{1/2}$]	R [-]
Richard, 2012 [4]	$7.82 \cdot 10^{-14}$	3.07	328.9	0.1
SH, 1996 [11,12]	$2.85 \cdot 10^{-13}$	2.88	259.3	0.1
SIZ, 2001 [13]	$4.51 \cdot 10^{-14}$	3.26	142.3	-
Blumenauer, 1993 [14]	$1.01 \cdot 10^{-14}$	3.50	158.1	-
Huth, 1979 [12,15]	$2.54 \cdot 10^{-12}$	2.70	-	0
Clark, 1974 [16,17,18]	$5.79 \cdot 10^{-11}$	2.25	-	-
IIW, 2012 (worst case) [19,20]	$5.21 \cdot 10^{-13}$	3.00	170.0	0
IIW, 2012 (characteristics) [19,20]	$3.00 \cdot 10^{-13}$	3.00	170.0	0
IIW, 2012 (mean) [19,20]	$1.80 \cdot 10^{-13}$	3.00	170.0	0
British Standard 7910, 2005 [12,21]	$5.22 \cdot 10^{-13}$	3.00	170.0	0
ASME, 2004 [12,22]	$9.39 \cdot 10^{-14}$	3.00	173.0	0
Demofonti, 2001 [23,24]	$1.70 \cdot 10^{-13}$	2.94	-	0.1

Figure 1 shows the crack propagation curves for the crack propagation parameters from Table 1. The lines are differentiated through the critical stress intensity factor K_{IC}, according to [4]. For evaluation the Paris law [1] is applied, see equation 1. One main difference between the data is the fact that the British standard [12, 21] uses a bilinear description of crack propagation. The comparison basically illustrates, that the incorporated parameters, such as the threshold value ΔK_{th}, the constant C and exponent m of the Paris law and the critical stress intensity factor K_{IC} exhibit significant scatter, whereas the values proposed by guidelines [12] or recommendations [19] should lead to a conservative assessment.

$$\frac{\mathrm{d}a}{\mathrm{d}N} = C \cdot \left(\frac{\Delta K}{\mathrm{MPa} \cdot \sqrt{\mathrm{mm}}} \right)^m \tag{1}$$

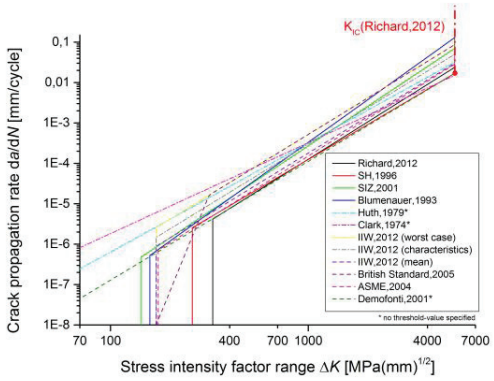

Fig. 1. Crack propagation curves from literature.

Crack growth testing is carried out on an electromagnetic resonance test machine. To this purpose, the FRACTOMAT and the testing machine are connected to a measurement amplifier to record the number of load cycles and the crack length simultaneously.

2.1. V-Notch

A single edge notch tension (SENT) specimen is manufactured by wire-eroding a V-notch into one edge of the specimen. Figure 2 shows the geometry of the specimen and the main dimensions. Two crack gauges are applied on both sides of the specimen surface. The first crack gauge is positioned at the V-notch to assure crack length measurement from the beginning of testing. Therefore, a smaller crack gauge with a nominal measuring length of 10 mm is used. On the opposite side a crack gauge with a nominal measuring length of 20 mm is applied, leaving a gap to the notch root. Due to the size of the specimen it is not possible to apply the gauge directly at the notch root and record the crack length from the very beginning; however, in this way it is assured that the crack propagation can be recorded also at later stages of testing.

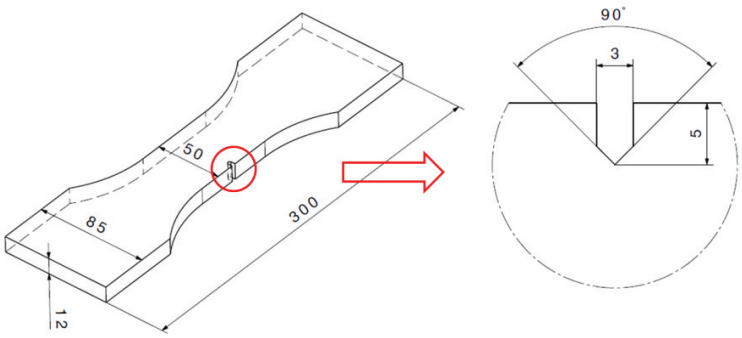

Fig. 2. SENT specimen with V-notch.

Before testing, the FRACTOMAT and the measurement amplifier are calibrated and the crack gauge area overlapping the notch is pre-cut to the notch root. The measured value after pre-cutting is taken into account as crack length offset in the numerical and analytical analysis afterwards. Two tests are carried out at constant amplitude loading (CAL) with stress ranges $\Delta\sigma = 150$ MPa and $\Delta\sigma = 100$ MPa, respectively and a synthesized test with variable amplitude loading (VAL) at both stress amplitudes is made (thereby giving a block load ratio of $R_b = 1.5$), all at a stress ratio $R = 0$. The VAL test starts at the higher stress level with block lengths at each

alternating stress level of 20.000 load cycles. Figure 3 shows the results of the two CAL tests compared to the VAL test. The diagram illustrates that the CAL test at $\Delta\sigma = 100$ MPa leads to a residual service life that is about four times longer than in the case of $\Delta\sigma = 150$ MPa. The VAL specimen exhibits a higher crack propagation rate at the beginning at $\Delta\sigma = 150$ MPa than the corresponding CAL specimen. This fact can be explained because the crack initiation stage at the CAL tested specimen is slightly longer (the specimens are notched, but not fatigue pre-cracked).

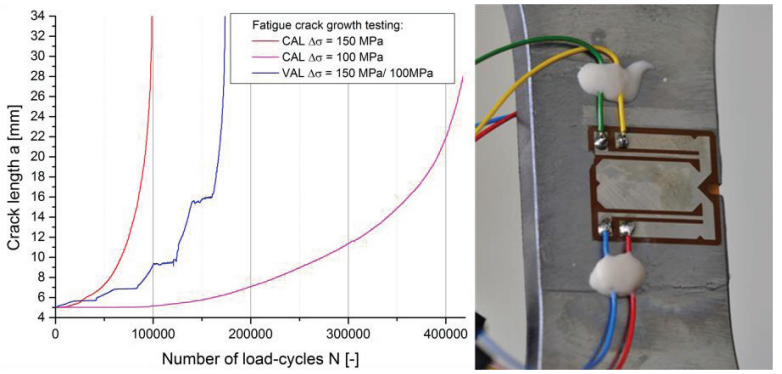

Fig. 3. a/N-curves of V-notch SENT specimen (left) and specimen with crack gauge (right).

Figure 4 shows the fracture surface of the VAL specimen, where the different stress levels can be clearly differentiated by the beach marks. The blocks with a stress range of $\Delta\sigma = 100$ MPa are visible as dark beach marks on the surface. In accordance with the number of applied blocks during testing, four dark beach marks can be observed.

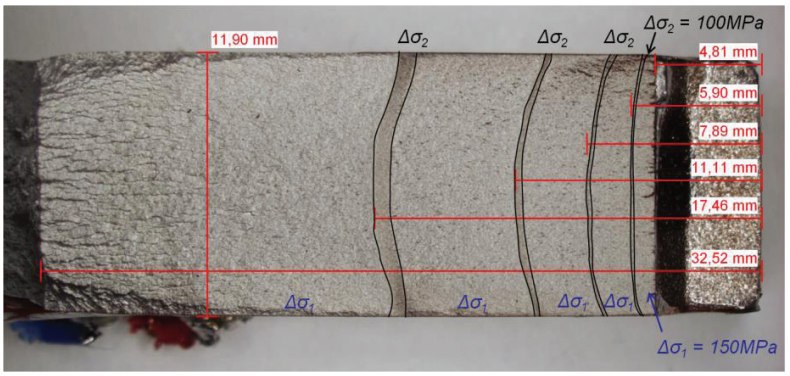

Fig. 4. Fracture surface of the V-notch SENT specimen.

The crack length at the end of each load sequence is measured in the light-optical microscope. Figure 4 illustrates that the crack extension at the edges of the specimen is influenced by the plane stress condition near the free surfaces. Table 2 summarizes the final number of load cycles measured in the crack growth experiments on the V-notch specimens.

Table 2. Fatigue crack growth test results for V-notch specimens

Specimen	Number of load cycles
CAL $\Delta\sigma$ = 150 MPa	99.600
CAL $\Delta\sigma$ = 100 MPa	415.000
VAL $\Delta\sigma$ = 150 / 100 MPa	173.300

2.2. SE-Notch

A surface crack tension (SCT) specimen (Figure 5) is manufactured by spark eroding a semi-elliptical notch with a depth of a_0 = 1 mm and a width of $2 \cdot c_0$ = 2.5 mm (giving a/c = 0.8) into the top surface in the center of the specimen. In the same manner as for the V-notch specimen, two CAL tests and one VAL test are performed. In contrast to the V-notch specimen, the crack growth in this case is a two-dimensional phenomenon; however, with crack gauges the crack propagation can only be measured along the surface. Again, the crack gauge is applied at a distance of a few millimeters to the notch root. Crack extension from the start of testing to the beginning of the crack gauge is assessed after testing by optical microscopy. Additionally, strain gauge measurements are performed to determine superimposed stresses due to the clamping of the specimens and their effect on the crack growth during testing. To this purpose, two strain gauges are applied in loading direction on each side of the specimen in 20 mm distance to the start notch.

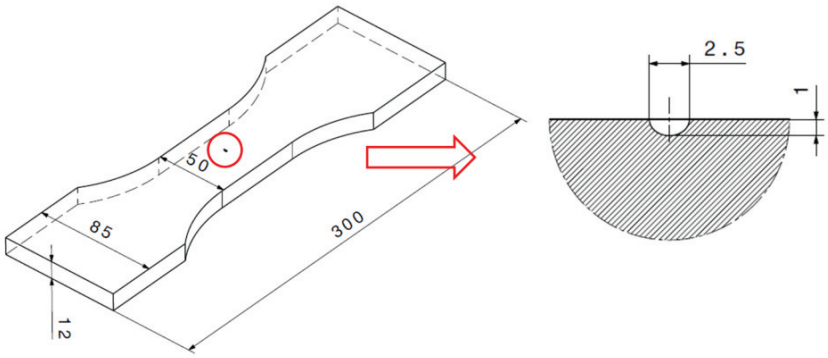

Fig. 5. Surface crack tension specimen with semi-elliptical notch.

Depending on the distortion of the specimens, the resulting stress distribution after clamping is more or less distinctive. Figure 6 depicts the measured stresses during clamping and the corresponding SE-notched specimen with two strain gauges. On the opposite side of strain gauge #1, strain gauge #3 is applied. Accordingly, strain gauge #4 is applied on the opposite side of strain gauge #2. In case of a highly distorted specimen, clamping tensile stresses up to 90 MPa are measured. The resulting strain gauge values indicate a superimposed static shell bending stress distribution of the specimen due to the clamping process.

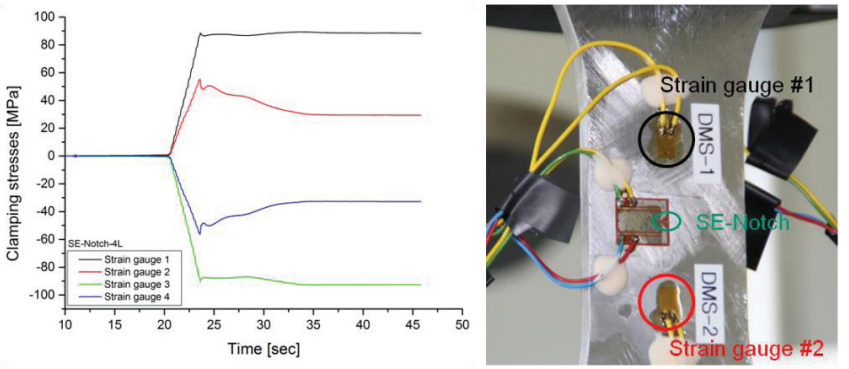

Fig. 6. Strain gauge measurements at clamping.

Similarly to the V-notch specimens, two CAL tests at $\Delta\sigma = 300$ MPa and $\Delta\sigma = 250$ MPa and a further VAL test are carried out. The stress amplitudes of the VAL test were 300 MPa and 200 MPa, respectively, with block lengths of 20.000 load cycles beginning with the higher load. As in the V-notch test, the block ratio is $R_b = 1.5$. The fracture surface depicted in Figure 7 illustrates the area of variable amplitude crack propagation A and forced rupture B.

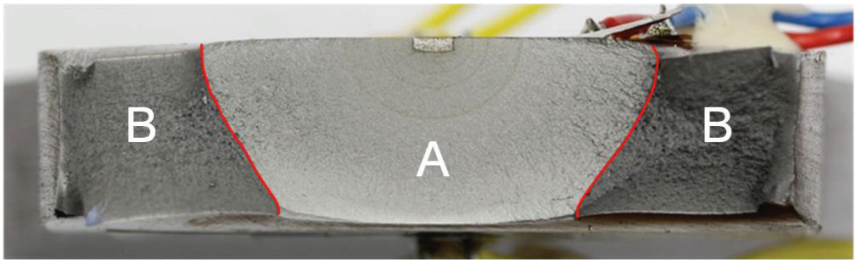

Fig. 7. Fracture surface with beach marks.

Figure 8 shows the results of the crack growth tests, in which the surface crack length $2c+2\Delta c$ depending on the number of load cycles is represented, and a detailed microscopy of the five beach marks under VAL. Due to the size restrictions of the crack gauges, the surface crack length is not measured from the beginning. The deviation of crack growth and start of crack growth measurement is visible as a step in the diagram. The crack length from crack gauge measurements and the crack lengths measured by microscopy show good agreement.

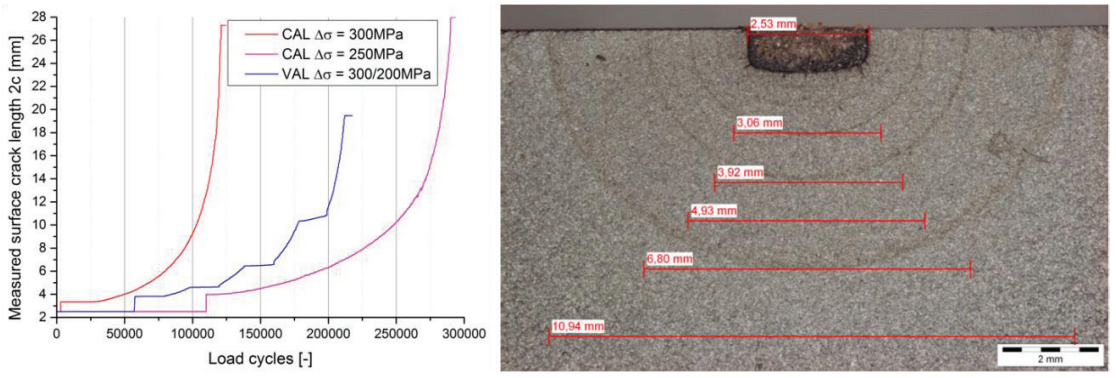

Fig. 8. Surface crack length 2c vs. number of load cycles (left), microscopy of beach marks for the VAL case (right).

The aspect ratio (crack depth to surface crack half-length) of the start notch increased during testing from $a/c = 0.8$ to $a/c = 0.92$ at the last beach mark. The fracture surface in Figure 8 shows symmetrical crack propagation along the surface. In Table 3, the final numbers of load cycles for the CAL tests and the VAL test are summarized.

Table 3. Fatigue crack growth test results for SE-notch specimens

Specimen	Number of load cycles
CAL $\Delta\sigma = 300$ MPa	121.000
CAL $\Delta\sigma = 250$ MPa	290.500
VAL $\Delta\sigma = 300 / 200$ MPa	212.000

Figure 8 illustrates a deviation of the required semi-elliptical shape of the starter notch due to manufacturing. However, the observation of the beach marks shows a semi-elliptical crack extension and seems to be not affected by the starter notch.

Crack propagation analysis

Estimation of crack propagation is a fundamental necessity for determining inspection intervals and remaining service life in damage tolerant design. In what follows, crack propagation analyses are conducted to compare numerical and analytical methods with experimental results. Different tools are used to study crack propagation for the specimens under investigation; in all cases, crack growth is calculated based on linear-elastic fracture mechanics (LEFM). The parameters C and m of the Paris law [1], are determined on the basis of the experimental crack growth results for the V-notch. All assessments used a start crack size of $a_0 = 5.05$ mm including an initial notch depth of $a_i = 5$ mm. The number of load cycles up to a_0 is taken into account by adding the load cycles of the particular fatigue crack growth test. The abort criterion is either the final crack length of the tested specimen or a critical stress intensity factor K_{IC}.

2.3. V-Notch

2.3.1. Analytical assessment

- *Procedure #1: Analytical calculation according to Tada [25]*

In [25] a number of empirical formulas of configuration correction factors (geometry functions) $F(a/W)$ for different types of common specimens are presented. In procedure #1, the formula for the correction factor for case of a single edge notch test specimen is applied in accordance with [25]. The results of the analytical estimation at different stress levels compared to fatigue crack growth tests are illustrated in Figure 9.

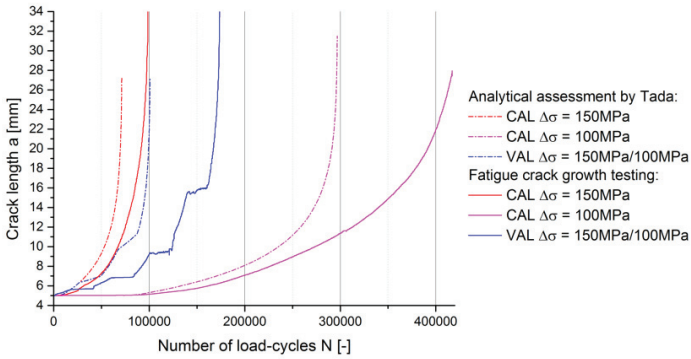

Fig. 9. Comparison of measured a/N-curve with analytical assessment according to Tada [25] for the V-notch specimens.

A comparison of the results indicates that all analytically determined numbers of load cycles for remaining service life are conservative compared to crack growth testing. The deviation of the analytical assessment at both CAL experiments (with stress ranges of 150 MPa and 100 MPa, respectively) was approximately 29%. The difference of the VAL estimation compared to fatigue crack growth testing is about 42%.

- *Procedure #2: Analytical assessment with nCode according to Murakami [26, 27]*

In procedure #2 a LEFM crack growth analysis by the aid of the software nCode Glyphworks is performed [26]. In this software tool, a flow diagram involving the specification of the load and fracture mechanics properties is built up to assess the remaining service life, see Figure 10. First, the stress definitions are connected to the crack growth analysis glyph. The latter one includes the growth law, the start and final crack length, material parameters, and the dimensions of the geometry together with the built-in function of geometry factor [28]. In case of the SENT (V-notch) specimen the geometry function according to Brown and Srawley [27, 29] is used for $0.2 \leq a/W \leq 0.8$. If $a/W < 0.2$, then a/W is set to 0.2 automatically, which leads to a higher stress intensity factor and more conservative values at the beginning of crack growth. In case of the SENT specimen with $W = 50$ mm, a crack length of $a < 10$ mm is handled as a 10 mm long crack.

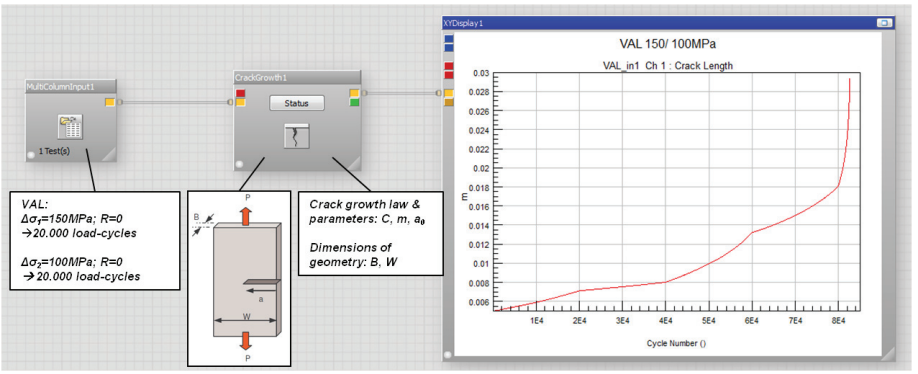

Fig. 10. Definition of a crack growth analysis in nCode.

Figure 11 shows the nCode assessment in comparison to the fatigue crack growth test results. The maximum deviation of about 48% is observed for the VAL specimen. As for procedure #1, the differences of the CAL estimations with approximately 38% at $\Delta\sigma = 150$ MPa and 36% at $\Delta\sigma = 100$ MPa were significantly lower.

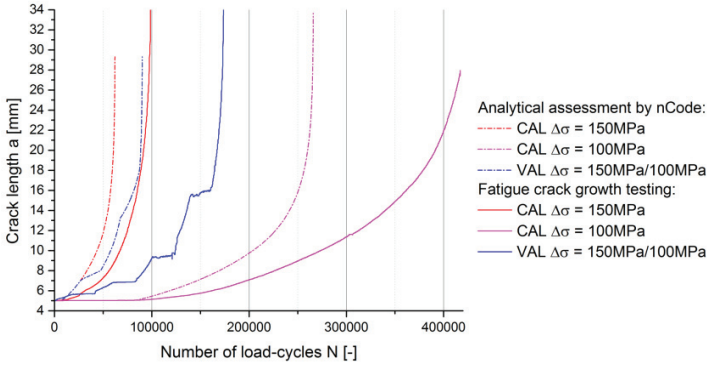

Fig. 11. Comparison of measured a/N-curve with analytical assessment according to [26, 27] for the V-notch specimens.

In all analytical assessments interaction effects due to VA loading are not considered, which may lead to more conservative results. To estimate the influence of VA loading on fatigue crack growth, several concepts exist. These concepts can be divided into global and cycle-by-cycle analyses. Whereas global models consider all loading cycles together, the cycle-by-cycle analyses take every cycle separately into account and accumulate them. For the latter, models for interaction effects exist [4, 7]. Table 4 shows the final number of load cycles for the two analytical calculation procedures compared to the results of testing; it can be seen that both calculation procedures result in a conservative estimate of the remaining service life.

Table 4. Comparison of final lifetime for V-notch

Specimen	Number of load cycles Experiment	Number of load cycles Calculation Procedure #1	Number of load cycles Calculation Procedure #2
CAL $\Delta\sigma$ = 150 MPa	99.600	71.200	62.100
CAL $\Delta\sigma$ = 100 MPa	415.000	296.700	265.900
VAL $\Delta\sigma$ = 150 / 100 MPa	173.300	100.700	90.100

Summarized, the most conservative results at both procedures are obtained at the VAL with approximately 42% deviation for calculation procedure #1 and about 48% for calculation procedure #2. Especially in case of VAL involving a change of the local behavior at the crack tip the assessment may lead to rather conservative results. In order to achieve more accurate results for VAL or load spectra including overloads, retardation effects and crack closure should be considered in further investigations.

2.3.2. *Numerical assessment*

Finite element (FE) methods are frequently used in engineering applications to assess the local conditions of complex structures. Franc2D [30, 31], as a two-dimensional crack propagation simulator, is used in this work to assess the stress intensity factor at the crack tip and the remaining service life of the V-notch specimen. The model and the mesh are built up with the pre-processor CASCA. For simplification the clamping surfaces are replaced by appropriate boundary conditions. In Figure 12 the stress distribution at a nominal maximum stress of σ_{max} = 150 MPa in x direction and the clamping conditions are illustrated. The left end of the model is clamped to consider the fixed clamping jaw. On the right side the load is applied and the edge is constrained in the y direction, thereby accounting for the moveable clamping jaw.

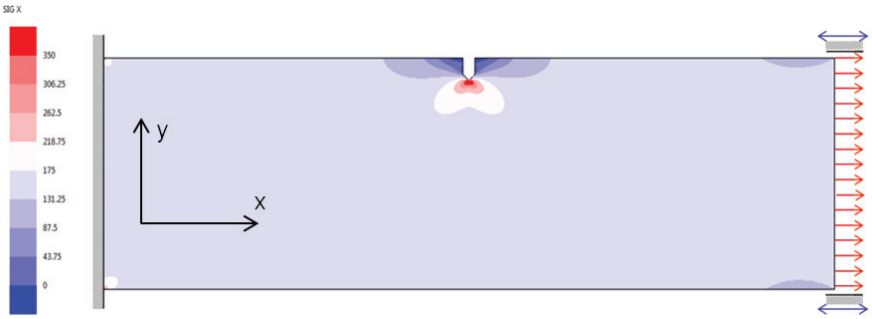

Fig. 12. Stress distribution in the SENT specimen σ_x at a nominal stress of σ_{max} = 150 MPa.

Based on this model, a LEFM analysis is performed. The material parameters are defined according to the analytical assessment procedures. The mesh consists of quadrilateral elements with a size of 0.5 mm x 0.5 mm along the crack ligament. At the beginning a start crack has to be defined. Due to the element size a start crack length a_0 = 0.05 mm from the notch root is defined, which gives a total crack length of 5.05 mm including the depth of the

notch. The local mesh size along the crack ligament is comparably fine to obtain sufficiently accurate stress intensity factors, see Figure 13.

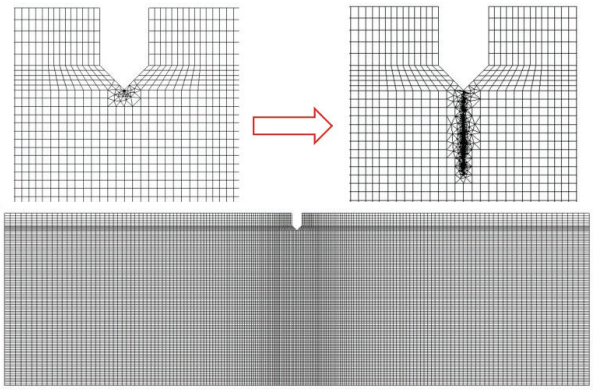

Fig. 13. Mesh of initial model and re-meshed crack

A crack growth increment of $\Delta a = 0.05$ mm for each step is chosen up to a final crack length of 15 mm; for larger crack sizes an increment of $\Delta a = 0.1$ mm is defined to reduce computation effort and time. The crack growth direction and the re-meshing of the crack tip are performed automatically. In this automatic procedure, the elements at the crack tip are deleted and re-meshed with triangular serendipity elements to consider the stress singularity. Figure 13 shows the meshed model and the re-meshed crack at lengths of $a = 5.05$ mm and 15 mm. Due to the small crack extension increment, a fine re-meshing of the crack is achieved. The results of the calculation compared to testing are illustrated in Figure 14.

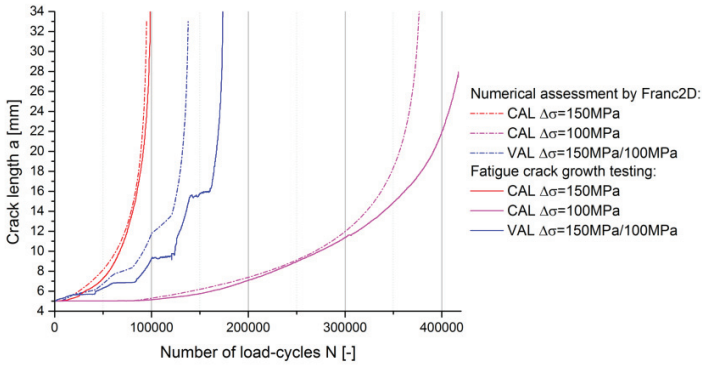

Fig. 14. Comparison of numerical predictions by Franc2D and experimentally obtained a/N-curves for the V-notch specimens.

The numerical calculations of the CAL generally agree well with the fatigue crack growth tests. Table 5 summarizes the results from Franc2D in comparison to the experimental results. An overall quite minor deviation of 5-10% is observed. The difference for the VAL specimen is about 20%, which can again be explained by retardation effects in the experiment when a load sequence changes from a high to a low stress level. Generally, the crack propagation rate is not that strong influenced by acceleration effects due to a low-high load sequence.

Table 5. Comparison of final lifetime for V-notch, experiment and numerical calculation

Specimen	Number of load cycles Experiment	Number of load cycles Numerical (Franc2D)
CAL Δσ = 150 MPa	99.600	94.900
CAL Δσ = 100 MPa	415.000	377.000
VAL Δσ = 150 / 100 MPa	173.300	137.900

2.4. SE-Notch

For the semi-elliptical (SE) notch, the crack growth calculations were performed in the software tool Cyclic Crack Growth Simulation *(CCGS)* [32] based on an analytical solution for the stress intensity factor for a semi-elliptical surface crack under shell bending and membrane stress given in section 6.2.4 of the IIW recommendations for fatigue design [19],

$$K = \left(\sigma_{\mathrm{mem}} + H \cdot \sigma_{\mathrm{ben}}\right) \cdot \sqrt{\frac{\pi a}{Q}} \cdot F_{\mathrm{s}}. \tag{2}$$

H, Q and F_{s} are geometry functions depending on the specimen and crack dimensions t, a, c; H and F_{s} depend additionally on the position along the crack front. The membrane stress σ_{mem} is due to the cyclic loading with load ratio $R = 0$ and oscillates between a minimum value of 0 and a maximum value given by the load stress range $\Delta\sigma$. The shell bending stress σ_{ben} is a superimposed static stress due to clamping, cf. Fig. 6. Hence, the cyclic SIF ranges for fatigue crack growth at the root (deepest) point A and the surface point C, respectively, are

$$\begin{Bmatrix} \Delta K_{\mathrm{A}} \\ \Delta K_{\mathrm{C}} \end{Bmatrix} = \Delta\sigma \cdot \sqrt{\frac{\pi a}{Q(a/c)}} \cdot \begin{Bmatrix} F_{\mathrm{s,A}} \\ F_{\mathrm{s,C}} \end{Bmatrix}, \tag{3}$$

and the load ratios accounting for the presence of a mean stress due to clamping are, again for points A and C,

$$\begin{cases} R_{\mathrm{app,A}} = \dfrac{K_{\mathrm{min,A}}}{K_{\mathrm{max,A}}} = \dfrac{H_{\mathrm{A}} \cdot \sigma_{\mathrm{ben}}}{\Delta\sigma + H_{\mathrm{A}} \cdot \sigma_{\mathrm{ben}}} \\ R_{\mathrm{app,C}} = \dfrac{K_{\mathrm{min,C}}}{K_{\mathrm{max,C}}} = \dfrac{H_{\mathrm{C}} \cdot \sigma_{\mathrm{ben}}}{\Delta\sigma + H_{\mathrm{C}} \cdot \sigma_{\mathrm{ben}}} \end{cases}. \tag{4}$$

The fatigue crack growth rate at points A and C is then calculated by

$$\begin{cases} \mathrm{d}a/\mathrm{d}N = C \cdot \left(\Delta K_{\mathrm{A}} + R_{\mathrm{app,A}} \cdot \Delta K_{\mathrm{th,0}}\right)^m \\ \mathrm{d}c/\mathrm{d}N = C \cdot \left(\Delta K_{\mathrm{C}} + R_{\mathrm{app,C}} \cdot \Delta K_{\mathrm{th,0}}\right)^m \end{cases} \tag{5}$$

Here, the expression $R_{\mathrm{app}} \cdot \Delta K_{\mathrm{th,0}}$ accounts for an increased crack growth rate at load ratios $R_{\mathrm{app}} > 0$ compared to $R = 0$, at which the parameters C and m have been determined; $\Delta K_{\mathrm{th,0}}$ denotes the threshold stress intensity factor at $R = 0$ and typically assumes values between 5.5 and 8 MPa√m for steel.

The results of the CCGS computations at different stress levels compared to the fatigue crack growth tests are illustrated in Figure 15 and Table 6. A marked influence of the superimposed static bending stress due to clamping ("distortion") is observed. For constant amplitude loading (CAL), the numerical prediction is significantly improved by including the clamping stress influence by means of the expression $R_{app} \cdot \Delta K_{th,0}$. For the variable amplitude case (VAL), the prediction including the clamping stress overpredicts the fatigue crack growth rate, whereas the model without clamping stress agrees very well with the measurement. This, however, is only because the VA blocks with higher loads induce compressive residual stresses in front of the crack that lead to a crack growth retardation during subsequent blocks with lower loads; the simple crack growth model used here does not account for this retardation mechanism.

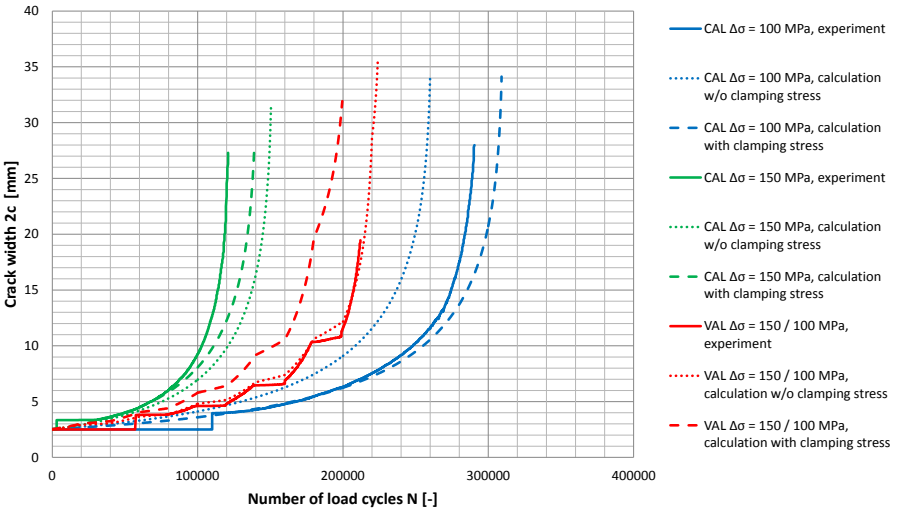

Fig. 15: Comparison of numerically and experimentally evaluated fatigue crack growth curves (crack width 2c vs. load cycles N).

Table 6. SE-notch results

Specimen	Number of load cycles Experiment	Number of load cycles CCGS with clamping stress	Number of load cycles CCGS without clamping stress
CAL Δσ = 150 MPa	121.000	139.000	150.500
CAL Δσ = 100 MPa	290.500	309.100	260.000
VAL Δσ = 150 / 100 MPa	212.000	199.500	224.000

3. Conclusion

Based on the experimental, analytical and numerical work the following conclusions can be drawn:

- The material parameters C and m, determined from fatigue crack growth testing of V-notch (SENT) specimens, match well to values for mild steel in literature.
- An assessment of the remaining service lifetime of the V-notch specimen at CAL and VAL is conservative compared to testing. A numerical computation of the crack propagation with Franc2D for CAL leads to a very good agreement with experiment, but however, as the results in this work are based on LEFM an application leads to a higher deviation in the VAL case due to missing retardation effects.
- The investigations of the SE-notch specimen with CCGS at CAL illustrate that a consideration of the clamping-induced bending stresses leads to a more accurate calculation of the remaining service life.

- The assessment at VAL including clamping stresses overestimates the crack propagation due to missing consideration of compressive residual stresses in front of the crack tip due to plasticity effects. The VAL estimation without clamping stresses shows good agreement with testing.
- The observation of the beach marks shows no influence due to the deviation of the semi-elliptical shape of the starter notch.

Acknowledgements

Financial support by the Austrian Federal Government (in particular from Bundesministerium für Verkehr, Innovation und Technologie and Bundesministerium für Wissenschaft, Forschung und Wirtschaft) represented by Österreichische Forschungsförderungsgesellschaft mbH and the Styrian and the Tyrolean Provincial Government, represented by Steirische Wirtschaftsförderungsgesellschaft mbH and Standortagentur Tirol, within the framework of the COMET Funding Programme is gratefully acknowledged.

References

[1] P.C. Paris, F. Erdogan, A critical analysis of crack propagation laws. In: Journal Basic Engineering 85 1963, p. 528-534
[2] R.G. Forman, S.R. Mettu. Behavior of surface and corner cracks subjected to tensile and bending loads in Ti-6Al-4V alloy. In: Fracture Mechanics: 22nd Symposium, Vol. 1 (Eds H.A. Ernst, A. Saxena, D.L. McDowell), ASTM STP 1131, American Society for Testing and Materials, Philadelphia 1992, 519-546.
[3] Maierhofer J, Pippan R, Gänser HP. Modified NASGRO equation for physically short cracks. Int J Fat 2014;59: 200-07.
[4] H.A. Richard, M. Sander, Ermüdungsrisse Erkennen sicher beurteilen vermeiden,2nd ed., Springer Vieweg, 2012.
[5] J. Schijve, Fatigue of structures and materials, 2nd ed, Springer, Berlin, 2009.
[6] M. Sander; H.A.Richard, Fatigue crack growth under variable amplitude loading Part I: experimental investigations. Fatigue Fracture of Engineering Materials and Structures, 2006, Vol.29; p. 291–301.
[7] M. Sander, H.A. Richard, Fatigue crack growth under variable amplitude loading Part II: analytical and numerical investigations. Fatigue Fracture of Engineering Materials and Structures, 2006, Vol.29; p. 303–319.
[8] M. Skorupa, Load interaction effects during fatigue crack growth under variable amplitude loading- a literature review. Part II: qualitative interpretation. Fatigue Fracture of Engineering Materials and Structures 22; 1998, p. 905-926.
[9] C. Bichler, R. Pippan, Effect of single overloads in ductile metals: A reconsideration. In Engineering Fracture Mechanics, 2007, Vol.74; p.1344-1359.
[10] Russenberger Prüfmaschinen AG, www.rumul.ch, 2015.
[11] S. Han, Rissfortschrittsverhalten von Baustählen in der Nähe des Ermüdungsschwellwertes, Shaker Verlag, 1996;8.
[12] Maschinenbau Forschungskuratorium, Fracture mechanics proof of strength for engineering components. 3rd ed. Frankfurt, VDMA Verlag; 2009.
[13] Stahl-Informations-Zentrum, Dokumentation 570 Grobblech-Herstellung und Anwendung, 1st ed, 2001.
[14] H. Blumenauer, G. Pusch; Technische Bruchmechanik, 3rd ed., Deutscher Verlag für Grundstoffindustrie, Leipzig, 1993.
[15] H. Huth, Berechnungsunterlagen zur Rissfortschritts- und Restfestigkeitsvorhersage rissbehafteter Großbauteile, ARGE Betriebsfestigkeit im VdEH, Bericht Nr. ABF06, 1979.
[16] D. Radaj, M. Vormwald, Ermüdungsfestigkeit Grundlagen für Ingenieure, 3rd ed., Springer, Berlin, 2007; p.415-416.
[17] K.-H. Schwalbe, Bruchmechanik metallischer Werkstoffe, Hander Verlag, Münschen, 1980.
[18] W.G. Clark, How fatigue crack initiation and growth properties affect material selection and design criteria, Metals Engng. Quart., 1974.
[19] A. Hobbacher, Recommendations for fatigue design of welded joints and components, IIW document IIW-1823-07, International Institute of Welding, 2008
[20] A. Hobbacher, Update of fracture mechanics chapters of the IIW fatigue design recommendations, International Institute of Welding, 2012.
[21] British Standard 7910, Guide to Methods for Assessing the Acceptability of flaws in metallic structures, British Standards Institution, 2005.
[22] ASME Boiler and Pressure Vessel Code, Section XI, Rules for Inservice Inspection of Nuclear Power Plant Components, American Society of Mechanical Engineers, 2004.
[23] G. Demofonti et al., High-strength steels in welded state for lightweight constructions under high and variable stress peaks, Final report EUR 19989, 2001.
[24] R.J.M. Pijpers, Fatigue strength of welded connections made of very high strength cast and rolled steels, doctoral thesis, Delft, 2011; p.84.
[25] H. Tada, Paul C. Paris, George R. Irwin, The stress analysis of cracks handbook, ASME Press, New York, 2000; p. 52-53.
[26] HBM nCode, Glyph Reference Guide, 2014; p. 713-729.
[27] Y. Murakami et al., Stress intensity factors handbook, Volume 1, Pergamon Press, Oxford, 1987, p. 9.
[28] HBM nCode, Crack Growth Stress Intensity Functions, 2010; p. 2.
[29] W.F. Brown, Jr., J.E. Srawley, Plane Strain Crack Toughness Testing of High Strength Metallic Materials, ASTM STP 410, 1966, p. 12.
[30] www.cfg.cornell.edu/software/software.htm. , Cornell University Fracture Group, 2015
[31] P.A. Wawrzynek, A.R. Ingraffea, FRANC2D A Two Dimensional Crack Propagation Simulator, User's Guide, Version 3.1, Cornell University, Ithaca, 1993.
[32] Cyclic Crack Growth Software (CCGS), http://www.mcl.at/forschung/software.html, 2015